Received: 10 February 2022 | Revised: 3 March 2022 | Accepted: 7 March 2022

DOI: 10.1002/prot.26334

RESEARCH ARTICLE

PROTEINS WILEY

Structure and function of an *N*-acetyltransferase from the human pathogen *Acinetobacter baumannii* isolate BAL_212

Noah R. Herkert | James B. Thoden | Hazel M. Holden

Department of Biochemistry, University of Wisconsin, Madison, Wisconsin, USA

Correspondence
Hazel M. Holden, Department of Biochemistry, University of Wisconsin, Madison, WI 53706, USA.
Email: hazel_holden@biochem.wisc.edu

Funding information
National Institutes of Health: R35 GM134643

Abstract

Acinetobacter baumannii is a Gram-negative bacterium commonly found in soil and water that can cause human infections of the blood, lungs, and urinary tract. Of particular concern is its prevalence in health-care settings where it can survive on surfaces and shared equipment for extended periods of time. The capsular polysaccharide surrounding the organism is known to be the major contributor to virulence. The structure of the K57 capsular polysaccharide produced by *A. baumannii* isolate BAL_212 from Vietnam was recently shown to contain the rare sugar 4-acetamido-4,6-dideoxy-D-glucose. Three enzymes are required for its biosynthesis, one of which is encoded by the gene H6W49_RS17300 and referred to as VioB, a putative *N*-acetyltransferase. Here, we describe a combined structural and functional analysis of VioB. Kinetic analyses show that the enzyme does, indeed, function on dTDP-4-amino-4,6-dideoxy-D-glucose with a catalytic efficiency of 3.9 x 10^4 M^{-1} s^{-1} (±6000), albeit at a reduced value compared to similar enzymes. Three high-resolution X-ray structures of various enzyme/ligand complexes were determined to resolutions of 1.65 Å or better. One of these models represents an intermediate analogue of the tetrahedral transition state. Differences between the VioB structure and those determined for the *N*-acetyltransferases from *Campylobacter jejuni* (PglD), *Caulobacter crescentus* (PerB), and *Psychrobacter cryohalolentis* (Pcryo_0637) are highlighted. Taken together, this investigation sheds new insight into the Type I sugar *N*-acetyltransferases.

KEYWORDS
4,6-dideoxyhexoses, 4-acetamido-4,6-dideoxy-D-glucose, 4-amino-4,6-dideoxy-D-glucose, *Acinetobacter baumannii*, carbohydrate, enzyme structure, *N*-acetyltransferase

1 | INTRODUCTION

Acinetobacter baumannii is an opportunistic Gram-negative bacterium that has recently emerged as a significant human health threat worldwide.[1,2] Due to the increasing rise of *A. baumannii* infections in hospital settings, and its extensive antibiotic resistance spectrum, it has been designated as

Abbreviations: CoA, Coenzyme A; dTDP, thymidine diphosphate; HEPES, *N*-2-hydroxyethylpiperazine-*N*′-2-ethanesulfonic acid; MES, 2-(*N*-morpholino)ethanesulfonic acid; Ni-NTA, nickel-nitrilotriacetic acid; TEV, Tobacco Etch Virus; Tris, *tris*-(hydroxymethyl) aminomethane.

X-ray coordinates have been deposited in the Research Collaboratory for Structural Bioinformatics, Rutgers University, New Brunswick, N. J. (accession nos. 7TXP, 7TXQ, and 7TXS).

a "red alert."[3] Indeed, in 2017, the World Health Organization published a global priority list for the development of new antibiotics and placed *A. baumannii* into the "Critical" category.[4] It belongs to the so-called "ESKAPE" group of pathogens, which include *Enterococcus faecium*, *Staphylococcus aureus*, *Klebsiella pneumonia*, *A. baumannii*, *Pseudomonas aeruginosa*, and *Enterobacter species*. Members of this group are becoming increasingly resistant to the bactericidal effects of antibiotics. Of particular concern is the ability of *A. baumannii* to survive for extended periods of time on hospital surfaces and equipment.[5,6] Strikingly, some clinical isolates of *A. baumannii* have been shown to remain viable for ~100 days under dry conditions.[6] Whereas a variety of glycans are thought to contribute to *A. baumannii* viability including the lipooligosaccharide, the capsular polysaccharide, and the exopolysaccharide poly-β-(1–6)-*N*-acetylglucosamine, it is thought that the capsular polysaccharide is the major contributor to virulence.[7] Indeed, in one study, it was demonstrated that isolates lacking the capsular polysaccharide did not cause infections.[8]

The structure of the K57 capsular polysaccharide produced by *A. baumannii* isolate BAL_212 from Vietnam was recently shown to contain the rare sugar 4-acetamido-4,6-dideoxy-D-glucose (also referred to as *N*-acetylviosamine or D-Qui4NAc).[9] The genes required for its biosynthesis (Scheme 1) were identified as *rmlA* (H6W49_RS17310), *rmlB* (H6W49_RS17315), *vioA* (H6W49_RS17305), and *vioB* (H6W49_RS17300), which encode for a thymidylyltransferase, a 4,6-dehydratase, a pyridoxal 5′-phosphate-dependent aminotransferase, and an *N*-acetyltransferase, respectively.[9] In this report, we describe a combined structural and functional investigation of the *N*-acetyltransferase encoded by the H6W49_RS17300 gene in *A. baumannii* isolate BAL_212 and hereafter referred to as VioB. Surprisingly, one of the three structures determined in this investigation revealed the presence of a tetrahedral transition state analogue trapped in the crystalline lattice. We also provide a comparison between the model of VioB with those structures previously reported for the *N*-acetyltransferases from *Caulobacter crescentus* and *Psychrobacter cryohalolentis*, which also contained either a trapped transition state analogue or intermediate, respectively.[10,11]

2 | MATERIALS AND METHODS

2.1 | Protein expression and purification

The gene encoding VioB from *A. baumannii* (strain BAL_212 KL57) was synthesized by Integrated DNA Technologies. It was cloned into

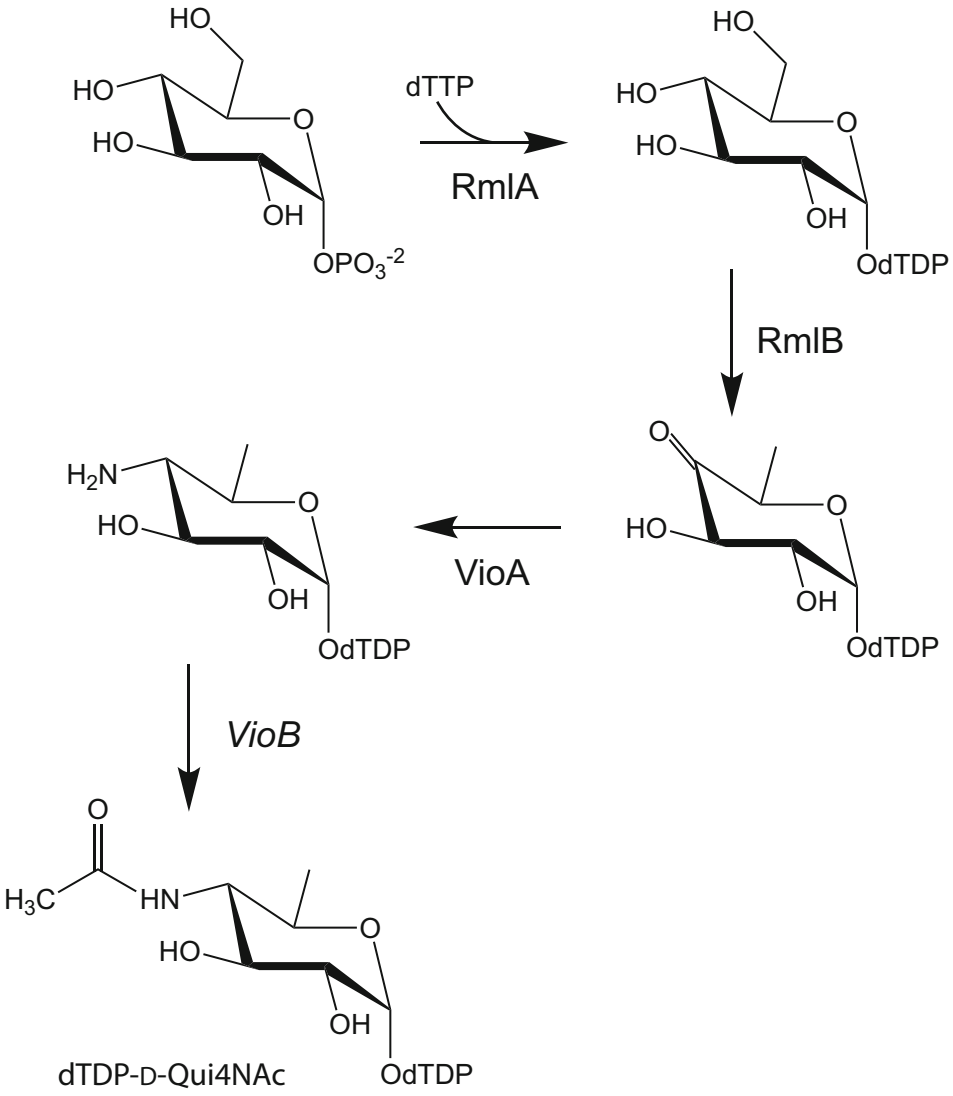

SCHEME 1 Predicted pathway for the biosynthesis of dTDP-D-Qui4NAc

TABLE 1 X-ray data collection and model refinement statistics

	dTDP-4-amino-4,6-dideoxy-D-glucose	Acetyl-CoA/dTDP	Intermediate analogue
Space group	***R*3**	***R*3**	***R*3**
Unit cell (*a*, *b*, *c*, [Å])	97.0, 97.0,73.3	97.4, 97.4, 72.8	97.9, 97.9, 73.0
Resolution limits (Å)	50.0–1.45 (1.55–1.45)[a]	50.0–1.65 (1.75–1.65)[a]	50.0–1.25 (1.35–1.25)[a]
Number of independent reflections	45094 (8089)	30576 (4811)	70527 (14096)
Completeness (%)	98.7 (96.8)	98.6 (96.3)	97.7 (94.5)
Redundancy	4.2 (2.9)	4.8 (3.2)	4.0 (2.6)
avg I/avg σ(I)	10.4 (3.0)	12.0 (3.0)	12.2 (3.0)
R_{sym} (%)[b]	6.9 (35.3)	6.1 (35.4)	6.1 (30.2)
R-factor (overall)%/no. reflections[c]	17.7/45094	17.4/30576	15.2/70527
R-factor (working)%/no. reflections	17.6/42854	17.2/28942	15.1/66908
R-factor (free)%/no. reflections	19.4/2240	20.4/1634	16.5/3619
Number of protein atoms	1591	1584	1618
Number of heteroatoms	248	260	373
Average B values			
Protein atoms (Å^2)	12.4	15.6	11.7
Ligand (Å^2)	11.2	24.2	12.4
Solvent (Å^2)	23.7	26.6	26.9
Weighted RMS deviations from ideality			
Bond lengths (Å)	0.010	0.008	0.010
Bond angles (°)	1.65	1.59	1.82
Planar groups (Å)	0.008	0.008	0.008
Ramachandran regions (%)[d]			
Most favored	99.0	99.0	99.0
Additionally allowed	1.0	1.0	1.0
Generously allowed	0.0	0.0	0.0

[a]Statistics for the highest resolution bin.
[b]$R_{sym} = (\Sigma|I - \bar{I}|/\Sigma I) \times 100$.
[c]*R*-factor $= (\Sigma|F_o - F_c|/\Sigma|F_o|) \times 100$ where F_o is the observed structure-factor amplitude and F_c is the calculated structure-factor amplitude.
[d]Distribution of Ramachandran angles according to PROCHECK.[13]

pET28t3g, a modified pET28b vector (Novagen), which yields a protein with an N-terminal polyhistidine tag as previously described.[12] It was also cloned into pET31b(+) to produce a protein with a non-cleavable C-terminal polyhistidine tag.

The constructs were utilized to transform Rosetta2(DE3) *Escherichia coli* cells (Novagen). Cultures were grown in lysogeny broth supplemented with kanamycin and chloramphenicol (both at 50 mg/L concentration) for pET28t3g-*viob* or ampicillin and chloramphenicol (100 mg/L and 50 mg/L concentration, respectively) for pET31b (+)-*viob* at 37°C with shaking until an optical density of 0.8 was reached at 600 nm. The flasks were cooled in an ice bath, and the cells were induced with 1 mM isopropyl β-D-1-thiogalactopyranoside and allowed to express protein at 21°C for 24 h.

The cells were harvested by centrifugation and frozen as pellets in liquid nitrogen. The pellets from the cell expressing the N-terminally tagged protein were subsequently disrupted by sonication on ice in a lysis buffer composed of 50 mM sodium phosphate, 20 mM imidazole, 10% glycerol, and 300 mM sodium chloride (pH 8.0). The lysate was cleared by centrifugation, and the enzyme was purified at 4°C utilizing Prometheus™ Ni-NTA agarose (Prometheus Protein Biology Products) according to the manufacturer's instructions. All buffers were adjusted to pH 8.0 and contained 50 mM sodium phosphate, 300 mM sodium chloride, and imidazole concentrations of 20 mM for the wash buffer and 300 mM for the elution buffer. Following Ni-NTA purification, the pooled protein samples were split in half. One half was dialyzed against 10 mM Tris–HCl (pH 8.0) and 200 mM NaCl. For the other half, the polyhistidine tag was removed by digestion with TEV protease. The TEV protease and remaining tagged proteins were removed by passage over Ni-NTA agarose, and the tag-free protein was dialyzed against 10 mM Tris–HCl (pH 8.0) and 200 mM NaCl. The C-terminally tagged protein was purified in the same manner as the N-terminally tagged enzyme. All constructs were concentrated to approximately 25 mg/mL based on an extinction coefficient of 3.1 $(mg/ml)^{-1}\ cm^{-1}$.

2.2 | Crystallizations

Crystallization conditions were surveyed by the hanging drop method of vapor diffusion using a sparse matrix screen developed in the Holden laboratory. Both the His-tagged and tag-free enzymes were tested for crystallization properties. The C-terminally tagged enzyme yielded X-ray diffraction quality crystals at room temperature using a precipitant containing 8%–12% poly(ethylene glycol) 8000, 200 mM LiCl, 5 mM dTDP-4-amino-4,-6-dideoxy-D-glucose, 5 mM CoA, and 100 mM MES (pH 6.0). All the crystals utilized in this investigation were initially grown under these conditions that included both the dTDP-sugar and CoA. X-ray data collection from 2-day old crystals and subsequent structural analyses revealed that the dTDP-sugar and CoA ligands were bound with low occupancy. Thus, in order to increase the occupancy of these ligands, crystals that were only 2 days old were then soaked in a ligand-free synthetic mother containing 15% poly(ethylene glycol) 8000, 200 mM LiCl, 200 mM NaCl, and 100 mM MES (pH 6.0). They were then transferred to solutions containing either 20 mM dTDP-4-amino-4,6-dideoxy-D-glucose, or 5 mM dTDP and 5 mM acetyl-CoA.

For X-ray data collection, the crystals were transferred to a cryoprotectant solution composed of either 24% poly(ethylene glycol) 8000, 250 mM LiCl, 250 mM NaCl, 20% ethylene glycol, 5 mM dTDP-4-amino-4,6-dideoxy-D-glucose, and 100 mM MES (pH 6.0) or 24% poly(ethylene glycol) 8000, 250 mM LiCl, 250 mM NaCl, 20% ethylene glycol, 5 mM dTDP, 5 mM acetyl-CoA, and 100 mM MES (pH 6.0).

The transition-state analogue model was obtained using crystals grown from 8%–12% poly(ethylene glycol) 8000, 200 mM LiCl, 5 mM dTDP-4-amino-4,6-dideoxy-D-glucose, 5 mM CoA, and 100 mM MES (pH 6.0), which were allowed to equilibrate for at least 2 weeks.

2.3 | X-ray data collection and processing

X-ray data sets were collected at 100 K utilizing a BRUKER D8-VENTURE sealed tube system equipped with Helios optics and a PHOTON II detector. These X-ray data sets were processed with SAINT and scaled with SADABS (Bruker AXS). Relevant X-ray data collection statistics are provided in Table 1.

2.4 | Structure solution and refinement

A partial model of the enzyme/intermediate analogue structure was initially built with MrBUMP[14] using the *N*-acetyltransferase domain of PglB from *Neisseria gonorrhoeae* (PDB entry 4 M98) as the starting model.[15] Iterative cycles of model-building with COOT[16,17] and refinement with REFMAC[18] led to a final X-ray model with an overall *R*-factor of 15.2%. The other structures were solved via difference Fourier techniques. Refinement statistics are presented in Table 1.

2.5 | Determination of kinetic parameters

The enzymatic activity of VioB was monitored spectrophotometrically by following the increase in absorbance at 412 nm due to the reaction of the sulfhydryl group of the CoA product with 5,5′-dithiobis-(2-nitrobenzoic acid). This results in a disulfide interchange leading to the formation of 5-thio-2-nitrobenzoic acid which possesses a characteristic absorbance at 412 nm with an extinction coefficient of 14 150 M^{-1} cm^{-1}.[19] Reactions were monitored continuously with a Beckman Coulter DU-640B spectrophotometer, and enzyme activities were calculated from the initial rates. Assay reaction mixtures were 100 μl in volume and contained, in addition to enzyme and substrates, 100 mM HEPES (pH 7.5) and 5 mM 5,5′-dithiobis-(2-nitrobenzoic acid).

To determine the steady-state kinetic parameters for dTDP-4-amino-4,6-dideoxy-D-glucose, acetyl-CoA was used at a concentration of 2.0 mM and the enzyme concentration of the tag-free version was 0.00055 mg/ml. The dTDP-4-amino-4,6-dideoxy-D-glucose concentration was varied from 0.025 mM to 6.0 mM ($K_M = 0.29 \pm 0.03$ mM, $k_{cat}/K_M = 39\,000 \pm 6000$ M^{-1} s^{-1}). These data were fitted to the equation: $v_0 = (V_{max}[S])/(K_M + [S])$ using Prism9 (GraphPad). The k_{cat} values per active site were calculated according to the equation: $k_{cat} = V_{max}/[E_T]$.

2.6 | Production of dTDP-4-amino-4,6-dideoxy-D-glucose

The ligand was synthesized and purified as previously reported from this laboratory.[20]

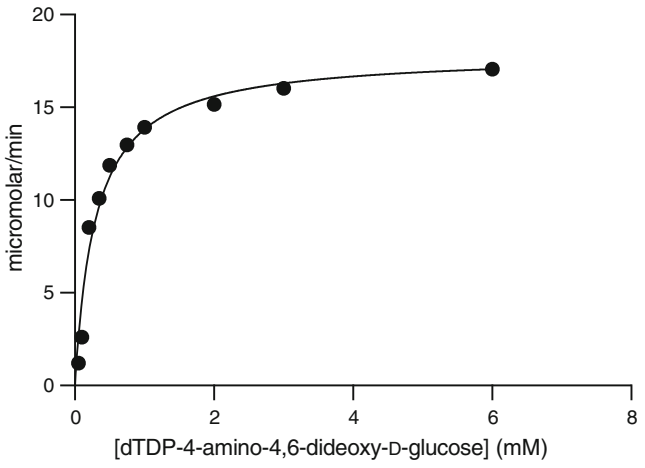

FIGURE 1 Plot of initial velocity versus substrate concentration. In presenting the data as we do, we are adhering to standard conventions in enzymology. Measuring velocities over a wide range of substrate concentrations allows us to obtain data that define both k_{cat} and k_{cat}/K_M well, which is not accomplished by measuring replicates at fewer different concentrations. The graph shown allows for a qualitative appreciation of the quality of the data; the quantitative goodness-of-fit to the Michaelis–Menten equation is given by the standard errors as described in Materials and Methods. The line shown is the calculated best fit

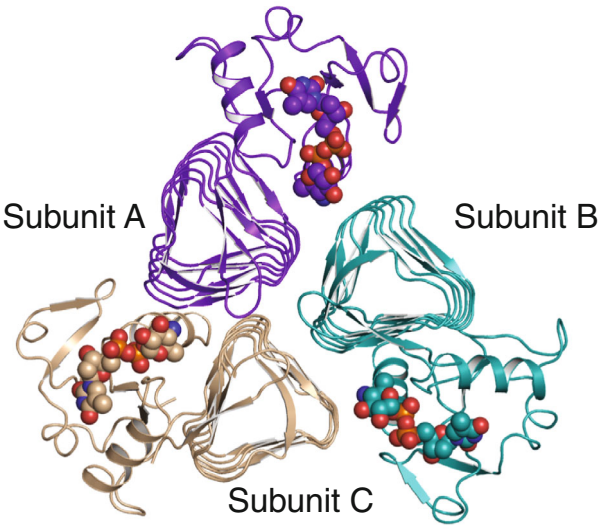

(A)

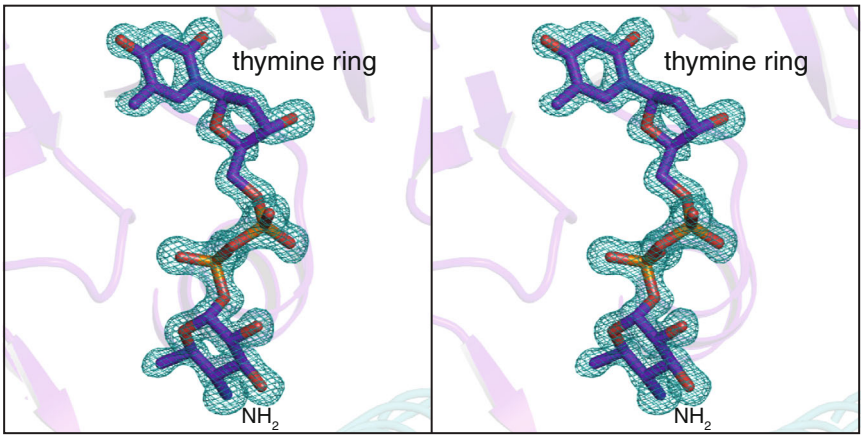

(B)

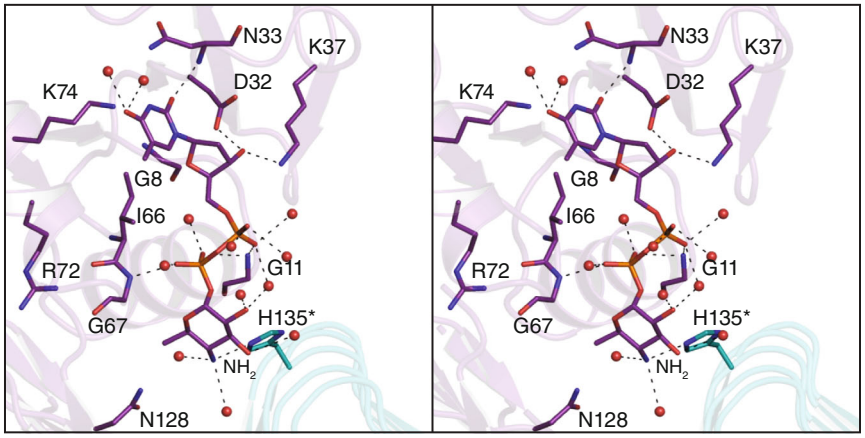

(C)

FIGURE 2 The molecular architecture of VioB. Shown in (A) is a ribbon representation of the trimer with the bound dTDP-sugar ligands depicted in space-filling representations. The observed electron density for the bound ligand is presented in (B). The electron density map, shown in stereo, was calculated with (F_o-F_c) coefficients and contoured at 3σ. The ligand was not included in the X-ray coordinate file used to calculate the omit map, and thus, there is no model bias. A close-up stereo view of the region surrounding the bound ligand is presented in (C). Ordered water molecules are displayed as red spheres. The dashed lines indicate possible hydrogen-bonding interactions within 3.2 Å. Note that the active site of VioB is shared by two subunits. Those amino acid residue labels marked by an asterisk belong to Subunit B. This figure and Figures 3–6 were prepared with PyMOL[28]

3 | RESULTS AND DISCUSSION

3.1 | Kinetic properties of VioB

The kinetic properties of VioB were determined via a continuous spectrophotometric assay. A plot of the initial velocity versus dTDP-4-amino-4,6-dideoxy-D-glucose is presented in Figure 1. VioB displays a $K_M = 0.29 \pm 0.03$ mM and a k_{cat}/K_M of 3.9 x 10^4 M^{-1} s^{-1} (±6000) for dTDP-4-amino-4,6-dideoxy-D-glucose. The catalytic efficiency of VioB is significantly less than that previously reported for the *N*-acetyltransferases from *C. jejuni* (using UDP-2-acetamido-4-amino-2,4,6-trideoxy-D-glucose, 2.0 × 10^7 M^{-1} s^{-1}), *C. crescentus* (using GDP-4-amino-4,6-dideoxy-D-mannose, 3.5 × 10^6 M^{-1} s^{-1}), or *P. cryohalolentis* (using UDP-2-acetamido-4-amino-2,4,6-trideoxy-D-glucose, 8.8 × 10^5 M^{-1} s^{-1}).[10,11,21]

3.2 | Structure of VioB

The structure of VioB in complex with dTDP-4-amino-4,6-dideoxy-D-glucose was solved to 1.45 Å resolution and refined to an overall *R*-factor of 17.7%. Previous investigations have shown that the nucleotide-linked sugar *N*-acetyltransferases function as trimers with *C*3 symmetry.[10,15,22–27] VioB packed in the crystalline lattice with its local three-fold rotational axis coincident to a crystallographic three-fold, thereby reducing the contents of the asymmetric unit to a single monomer. A ribbon representation of the trimer is displayed in Figure 2A. The observed electron density for the polypeptide chain backbone was continuous from Met 1 to Glu 209. Likewise, the electron density corresponding to the dTDP-sugar was unambiguous as can be seen in Figure 2B.

Each subunit folds into two distinct motifs formed by Met 1 to Phe 87 and Ala 88 to Glu 209. The N-terminal globular domain is dominated by a five-stranded mixed β-sheet flanked on either side by an α-helix. The architecture of the C-terminal domain consists of a β-helix composed of seven turns. Pro 201, which adopts a *cis* conformation, is located in the last turn of the β-helix (Gly 199 to Ala 202).

A close-up stereo view of the binding pocket for dTDP-4-amino-4,6-dideoxy-D-glucose is provided in Figure 2C. The thymine ring is anchored into the active site by the backbone amide of Asn 33 (Subunit A) and two water molecules. The ribosyl group, which adopts the C2′-*endo* pucker, participates in hydrogen bonding interactions with the side chains of Asp 32 and Lys 37 (Subunit A).

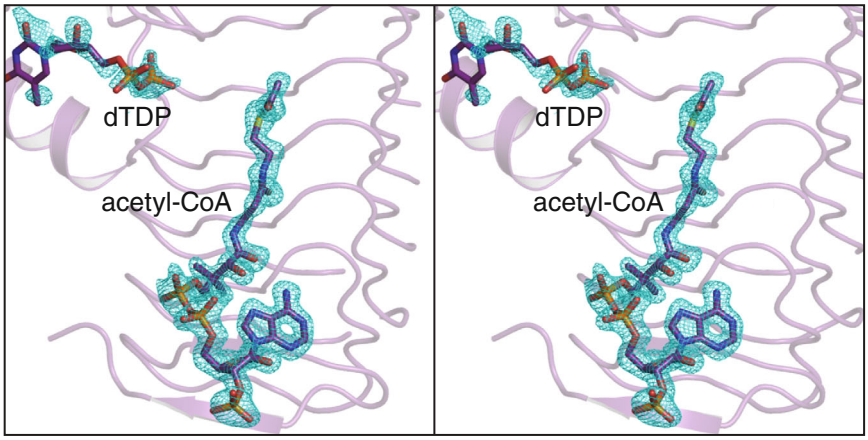

(A)

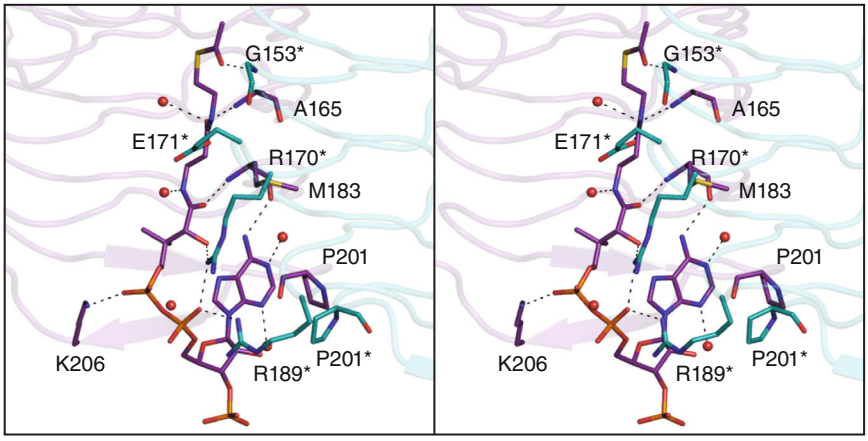

(B)

FIGURE 3 Structure of VioB in complex with dTDP and acetyl-CoA. The electron density map, shown in stereo in (A) was calculated with (F_o-F_c) coefficients and contoured at 3σ. Those amino acid residues lying within 3.2 Å of the acetyl-CoA cofactor are displayed in stereo in (B). Ordered water molecules are drawn as red spheres, and possible hydrogen-bonding interactions between the ligand and the protein are indicated by the dashed lines

The pyrophosphoryl group does not interact with side chains, but rather with water molecules and the backbone amides of Gly 11 and Gly 67 (Subunit A). His 135, contributed by Subunit B, lies within 2.7 Å of the C-4′ amino group. In addition to this hydrogen bond, there are five ordered water molecules that lie within 3.2 Å of the pyranosyl moiety.

The next structure determined in this investigation was that of the enzyme complexed with dTDP and acetyl-CoA. The model was refined to an overall *R*-factor of 17.4% at 1.65 Å resolution. Again, there was one molecule in the asymmetric unit. Shown in Figure 3A are the electron densities corresponding to the bound ligands. The electron density for the dTDP ligand was weak, whereas that for the acetyl-CoA was unambiguous. A stereo view of the acetyl-CoA binding pocket, which is positioned between subunits, is provided in Figure 3B. The side chains of Lys 206 (Subunit A), Arg 170 (Subunit B), and Arg 189 (Subunit B) serve to neutralize the negative charges on the phosphoryl oxygens of CoA, and the side chain of Glu 171 (Subunit B) forms a hydrogen bond with the nitrogen in the aminoethanethiol unit. Additional interactions between the cofactor and the protein are provided by the backbone amide groups of Ala 165 and Met 183 in Subunit A and Gly 153 in Subunit B. Five ordered water molecules also surround the ligand.

The third model of VioB solved in this investigation utilized X-ray data from crystals that had equilibrated under the original crystallization conditions (5 mM dTDP-4-amino-4,6-dideoxy-D-glucose and 5 mM CoA) for greater than 2 weeks. The model was refined to an overall *R*-factor 15.2% at 1.25 Å resolution. Shown in Figure 4A is the electron density observed in the active site. Strikingly, a tetrahedral adduct was obtained with the crosslinking group being $CHCH_3$. This phenomenon was first observed in our structural investigation of GDP-perosamine *N*-acetyltransferase from *C. crescentus*.[10] In that case, the crystals were grown using poly(ethylene glycol) as the precipitant, which is notorious for being contaminated with peroxides and aldehydes such as acetaldehyde.[29] It was proposed that the C-4′ amino group of the sugar attacked the carbonyl carbon of the contaminating acetaldehyde to form a tetrahedral intermediate. This intermediate was thought to collapse to a Schiff base, which was subsequently attacked by the sulfhydryl group of CoA. Likewise, the crystals of VioB were grown in the presence of poly(ethylene glycol) 8000 suggesting that the same chemistry had occurred. Given that the crystals were several weeks old before they were subjected to X-ray data collection, this most likely allowed for the development of the tetrahedral intermediate analogue. A close-up view of the region surrounding the tetrahedral adduct is presented in Figure 4B. The

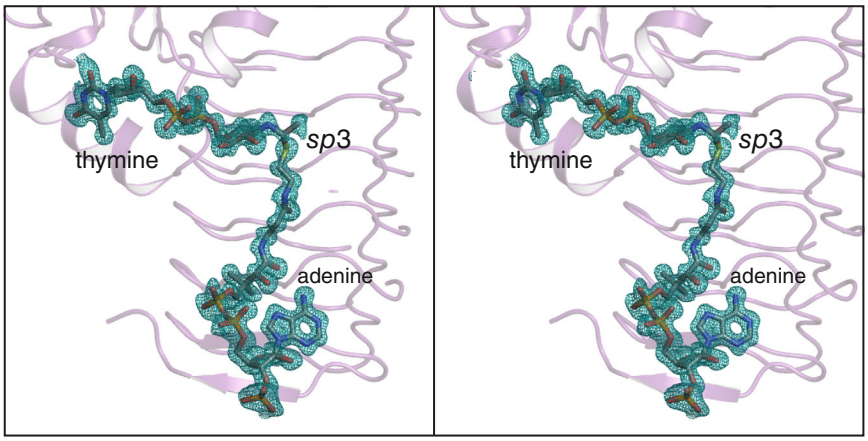

(A)

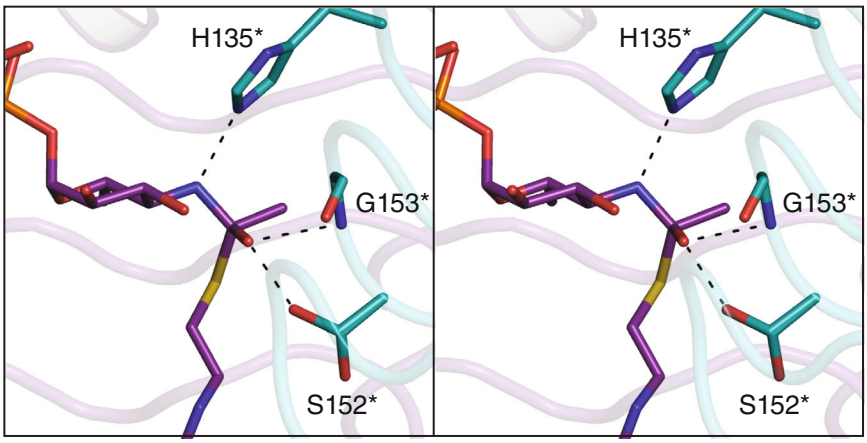

(B)

FIGURE 4 Structure of the VioB tetrahedral intermediate analogue. The observed electron density for the intermediate analogue is shown in stereo in (A). It was calculated with (F_o-F_c) coefficients and contoured at 3σ. Presented in stereo in (B) is a close-up view surrounding the tetrahedral intermediate model with potential hydrogen bonds to the oxyanion represented by the dashed lines

position of His 135 suggests that it functions as the active site base to abstract a proton from the C-4′ amino nitrogen. Most likely the backbone amide of Gly 153 provides stabilization of the oxyanion that forms during catalysis. Interestingly, in the model of VioB tetrahedral intermediate, Ser 152 adopts two distinct conformations, one of which would lie within hydrogen-bonding distance to the developing oxyanion at the transition state.

3.3 | Comparison of the VioB structure with other family members

One of the first molecular models of a monofunctional sugar *N*-acetyltransferase to be reported was that of PglD from *Campylobacter jejuni*.[22] This enzyme catalyzes the acetylation of UDP-2-acetamido-4-amino-2,4,6-trideoxy-D-glucose. The α-carbons for VioB and PglD correspond with a root-mean-square deviation of 1.8 Å. Our subsequent investigation of GDP-perosamine *N*-acetyltransferase (PerB) from *C. crescentus* revealed the presence of a trapped transition state analogue in the active site as mentioned above.[10] The α-carbons for VioB and PerB superimpose with a root mean square deviation of 1.4 Å. And recently, the structure of Pcryo_0637 from *P. cryohalolentis* was reported from this laboratory.[11] It utilizes the same substrate as PglD. Remarkably, in one of the Pcryo_0637 structures, a true tetrahedral intermediate rather than analogue was trapped in the active site. The α-carbons for VioB and Pcryo_0637 correspond with a root mean square deviation of 2.3 Å.

Shown in Figure 5A is a superposition of the α-carbons for VioB, PerB, Pcryo_0637, and PglD. All adopt a bilobal-type structure with approximately the first 90 residues folding into a globular domain dominated by a five-stranded mixed β-sheet. This domain is followed by a classical left-handed β-helix motif. Whereas VioB, PerB, and PglD are approximately the same size, Pcryo_0637 has two insertions (Leu 25 to Ile 36 and Ile 63 to Asp 66) in the N-terminal global domain and an insertion in the β-helix motif (Thr 180 to Pro 184) as indicated in Figure 5A.

An amino acid sequence alignment of these proteins, all of which belong to the Class I sugar *N*-acetyltransferases, is

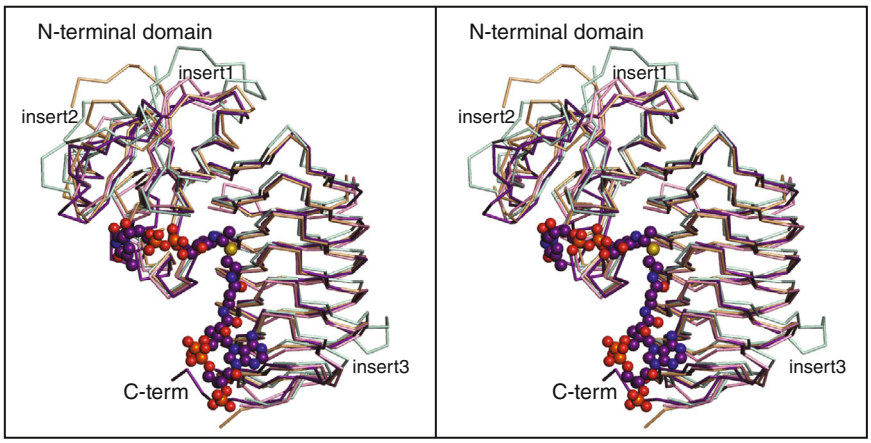

(A)

```
VioB    ---------MKELIIVGAGGHGNEISWLAKRCGRVVRGFLDNTVEKQGTFIRDI----PV 47
PerB    MGAASASLAIGGVVIIGGGGHAKVVIESLRACGETVAAIVDADPTRRA--VLGV----PV 54
0637    --------MSKVFAVYGASGCGRSLMPVANEQLR----ILEGDTDSQIVFIDDALDDNIT 48
PglD    ------MARTEKIYIYGASGHGLVCEDVAKNMGYKECI--------------------F 33
                     . : *..* .        .

VioB    LGTL------DECS-KFTDCDFVIAIGSPRARKKIIEHFFPEGEFTFATLIDPTATIGEN 100
PerB    VGDDLAL---PMLR-EQGLSRLFVAIGDNRLRQKLGRKA-RDHGFSLVNAIHPSAVVSPS 109
0637    VNGYTAMNYTKFKSIKNDDKFVLIAIANSSIRQKIADKL-VKDGISLWTVQGMTTLIMDE 107
PglD    LDDFKGM---KFES-TLPKYDFFIAIGNNEIRKKIYQKI-SENGFKIVNLIHKSALISPS 88
        :.                  ..:**..   *:*:  :   .  :.: .    :: :  .

VioB    IHIEE--GTMICAGGILTVDVKLGKHCIVNTNAVLSHGVILGDYVTVAPNASISGDVSLG 158
PerB    VRLGE--GVAVMAGVAINADSWIGDLAIINTGAVVDHDCRLGAACHLGPASALAGGVSVG 167
0637    VSIDA--GAALSPFVTIAANVTIGKCFHANLYSYVEHDCIIGDYVTFAPRVSCNGNIHIH 165
PglD    AIVEENAGILIMPYVVINAKAKIEKGVILNTSSVIEHECVIGEFSHVSVGAKCAGNVKIG 148
          :    *  :     : ..  : .    *  : :.*   :*    ..      *.: :

VioB    NIVEIGANATIREK-----VSVQDGAMVGMGSVVIRNILSNQVVVGNPAKLLKVIE 209
PerB    ERAFLGVGARVIPG-----VTIGADTIVGAGGVVVRDLPDSVLAIGVPAKIKGDRS 218
0637    DHAYIGTGAVIKQGTPDKPLIIGKGAIVGMGAVVTKEVPAGAVVIGNPARLLNK-- 219
PglD    KNCFLGINSCVLPN-----LSLADDSILGGGATLVKNQDEKGVFVGVPAKRM---- 195
        .   :* .: :        : :  .:::* *..: ::     : :* **:
```

(B)

FIGURE 5 Comparison of VioB, PerB, Pcryo_0637, and PglD. Shown in (A) is a stereo representation of the ribbon drawings for VioB, PerB, Pcryo_0637, and PglD depicted in violet, wheat, cyan, and pink, respectively. An amino acid sequence alignment for these enzymes is provided in (B). Conserved residues are highlighted in red

presented in Figure 5B. Of the 16 absolutely conserved residues among these *N*-acetyltransferases, nine are glycines. Gly 8 and Gly 11 are likely conserved given their location in the active site cleft. Specifically, the α-carbon of Gly 8 is only 3.8 Å away from the endocyclic oxygen of the dTDP ribose as shown in Figure 2C. This region simply cannot accommodate a larger side chain. This is equally true for Gly 11 with its α-carbon located within 3.9 Å of β-phosphoryl oxygen of the ligand (Figure 2C). Gly 106 is the third residue in Type II turn formed by Glu 104 and Thr 107. The peptidic nitrogen of this residue forms a hydrogen bond with the carbonyl oxygen of Ala 88 which resides in the random coil region connecting the N-terminal globular domain to the left-handed

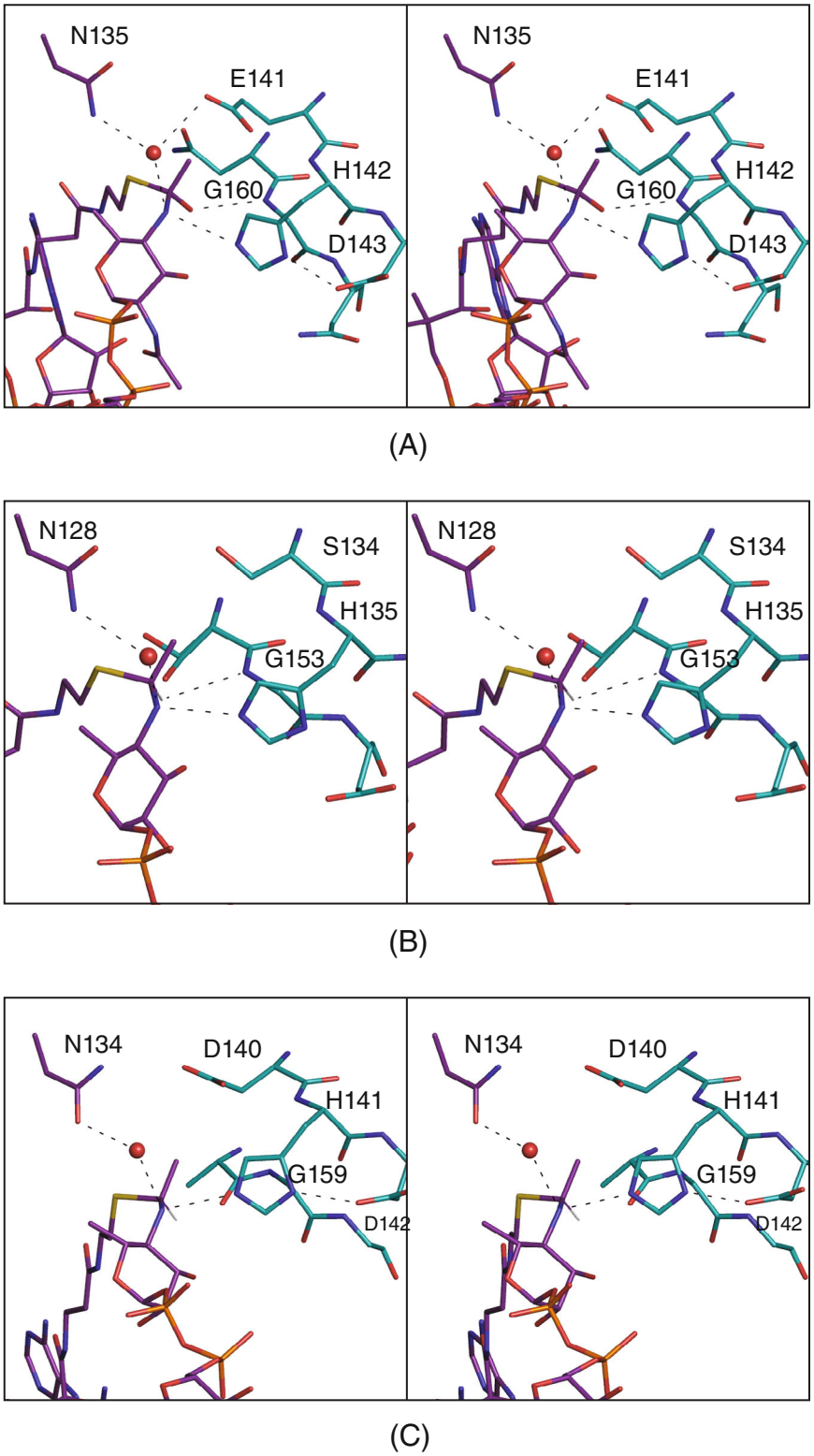

FIGURE 6 Comparison of the tetrahedral intermediates in Pcryo_0637, VioB, and PerB. The regions surrounding the tetrahedral intermediates observed in Pcryo_0637, VioB, and PerB are shown in stereo in (A), (B), and (C), respectively

β-helix motif. Note that the α-carbon of Gly 106 is located at 3.9 Å of the β-carbon of Phe 87. Any larger side chain would significantly perturb the tertiary structure of the enzyme. Gly 153 resides within 3.6 Å of His 135, the presumed catalytic base. A larger side chain would alter its position considerably in the active site cleft. Gly 182 is the first residue in a Type II turn located in the β-helix. Its α-carbon resides within 3.3 Å of the carbonyl oxygen of the pantothenic acid portion of CoA. The conserved Gly 184 is located in the third position of this Type II turn, and importantly, both the backbone peptidic nitrogen and the carbonyl group of Met 183 hydrogen bond with the carbonyl oxygen of the pantothenic acid portion and the NH_2 group of the adenine ring of the CoA, respectively (Figure 3B). The integrity of this turn is most likely critical for proper cofactor binding. Finally, Gly 199 initiates another turn that also contains the conserved Pro 201. This is the reverse turn that in certain *N*-acetyltransferases undergoes a conformational change upon CoA binding. It can be speculated that this conserved glycine is required for such flexibility. The reasons for the conservation of Gly 140 and Gly 164 are not apparent.

The two conserved charged residues, Arg 72 and Lys 74, are located near the active site. Specifically, the side chain of Lys 74 resides near the thymine ring of the bound ligand, whereas the guanidinium moiety of Arg 72 serves to bridge the carbonyl oxygens of Ile 66 and Gly 67 which, in turn, abut the β-phosphoryl group of the ligand (Figure 2C). His 135 is conserved because it functions as the catalytic base as discussed below. The conservation of Ala 65 and Asn 128 is not immediately obvious.

Previously, it was proposed that a carboxylic acid-containing residue following the histidine, either an aspartate or glutamate, either serves to increase the pK_a of the general base or to play a role in its proper positioning.[10,22,23] In the case of VioB, the residue following His 135 is glycine, thereby shedding doubt as to the need for a catalytic His/Glu(Asp) dyad for activity among the Type I *N*-acetyltransferases. Of interest is the conserved proline at the C-terminus (Pro 201 in VioB). From previous investigations, it has been shown that there is a *trans* to *cis* conformational change of this conserved proline upon CoA binding.[22,23] Specifically, in the absence of CoA, domain swapping occurs with the proline in the *trans* conformation, thereby allowing the last C-terminal β-strand of the β-helix to reach over to another subunit in the trimer. It is not known whether this same transition occurs in PerB because the structure of the enzyme is not known in the absence of CoA. Surprisingly, this *trans* to *cis* change does not occur in VioB where Pro 201 adopts the *cis* conformation regardless of the presence or absence of CoA.

In the first X-ray crystallographic analysis of PglD reported in 2008, molecular modeling was utilized to address the structural features involved in the reaction mechanism of the enzyme since it was not possible to obtain the enzyme/UDP-sugar complex.[22] On the basis of these insightful experiments, it was suggested that the conserved histidine (His 125 in PglD) functions as the catalytic base to abstract a proton from the sugar C-4′ amino group of the sugar, which was further supported by site-directed mutagenesis experiments. Additionally, His 125 was thought to be activated by its close proximity to the side chains of Glu 124 and Glu 126. It was also hypothesized that the sugar amino group enters the active site in its unprotonated form, which was subsequently validated in studies conducted by this laboratory on PerB.[10] Finally, the transition state model suggested that the tetrahedral intermediate would adopt the *S* absolute configuration, that the oxyanion would be stabilized by a hydrogen bond from the backbone amide of Gly 143, that the C-4′ amino nitrogen would hydrogen bond to Asn 118 via a water molecule, and that this interaction would aid in the stabilization of the tetrahedral intermediate.

These features can now be structurally addressed on the basis of the tetrahedral intermediates determined by this laboratory. Shown in stereo is Figure 6A is a close-up stereo view of the region surrounding the true tetrahedral intermediate in Pcryo_0637. Indeed, the intermediate adopts the *S* configuration, the oxyanion is stabilized by the backbone peptidic group of Gly 160, and the C-4′ amino nitrogen lies within 3.2 Å of His 142 and a water molecule, which, in turn, hydrogen bonds to Asn 135. As predicted for PglD, His 142 is positioned between two carboxylate side chains (Glu 141 and Asp 143). Several of these features are not conserved in either VioB or PerB, however. Indeed, in VioB, the conserved histidine (His 135) is not surrounded by carboxylate side chains but rather by Ser 134 and Gly 153. The water bridging the nitrogen of the tetrahedral intermediate to the asparagine residue (Asn 128) is present, though, as shown in Figure 6B. Strikingly, in PerB, the conserved histidine is surrounded by carboxylate containing side chains (Figure 6C), the water bridging, the nitrogen of the tetrahedral intermediate to the asparagine residue is conserved, but the backbone peptidic nitrogen of Gly 159 is not in the proper position to provide a positive charge to the oxyanion of the intermediate. It appears that the only truly conserved features among these three transition state intermediates (or analogues) are the positions of the catalytic histidines and the presence of water molecules that bridge the nitrogens of the intermediates to the carboxamide groups of the strictly conserved asparagine residues (Figure 6A–C). As noted above, VioB displays a significantly lower catalytic efficiency than PerB, PglD, and Pcryo_0637. This may be, in part, due to the lack of carboxylate-containing side chains surrounding the catalytic histidine that have been proposed to increase its p*K*a.

4 | CONCLUSION

In summary, we have demonstrated biochemically that VioB from *A. baumannii* isolate BAL_212 catalyzes the acetylation of dTDP-4-amino-4,6-dideoxy-D-glucose to yield dTDP-4-acetamido-4,-6-dideoxy-D-glucose. Acetyl-CoA serves as the two-carbon source. VioB demonstrates a catalytic efficiency of $3.9 \times 10^4\ M^{-1}\ s^{-1}$, which is significantly reduced compared to enzymes such as PglD, which displays a catalytic efficiency of $2.0 \times 10^7\ M^{-1}\ s^{-1}$. Indeed, the high catalytic efficiency of PglD suggests, according to diffusion theory, that it is nearing its evolutionary endpoint, which is not the case for VioB.

In all Type I sugar *N*-acetyltransferases studied thus far, there is a conserved proline that resides in the final turn of the β-helix motif. To

date, this proline in the Type I family members has been shown to undergo a *trans* to *cis* conformational change upon CoA binding. In the case of VioB, however, the proline adopts the *cis* conformation regardless of the presence or absence of the cofactor. Additionally, it has been suggested that a conserved dyad, namely the catalytic histidine, followed by either an aspartate or a glutamate, was important for catalysis. Surprisingly, the residue following the catalytic histidine in VioB is a glycine. This change may explain, in part, the reduced catalytic efficiency of VioB in comparison with other members of the Type I sugar *N*-acetyltransferases.

How common is 4-acetamido-4,6-dideoxy-D-glucose in the microbial world? It is not clear, but the first published report of its existence was in 1959 from *E. coli*.[30] Since that time, there have been sporadic reports of the sugar being isolated from the O-antigens of *Hafnia alvei* 1205, *A. baumannii*, *Pseudomonas fluorescens*, *Cellulophaga tyrosinoxydans*, and *Aeromonas hydrophila*.[31–36] An elegant biochemical characterization of the sugar *N*-acetyltransferase from *E. coli* O7 was described in 2007.[37] The kinetic parameters for the *E. coli* enzyme were similar to those reported here for VioB (K_M of 0.14 mM and a k_{cat}/K_M of 1.1×10^4 M^{-1} s^{-1}), and interestingly, the *N*-acetyltransferase from *E. coli* demonstrated catalytic activity over a temperature range of 4 to 65°C.

Other than these published reports, however, there remains a paucity of biological information regarding the presence and role of 4-acetamido-4,6-dideoxy-D-glucose. Indeed, whether 4-acetamido-4,-6-dideoxy-D-glucose is important for bacterial virulence is unknown at the present time. What is known, however, is that in some strains of *A. baumannii*, it has been found in either the O-antigen or in the capsular polysaccharide.[9,33] *A. baumannii* is an opportunistic pathogen responsible for nosocomial infections worldwide, and it is becoming increasingly resistant to the current arsenal of antibiotics. In light of this, a thorough understanding of its glycoconjugates and the enzymes responsible for their biosynthesis is critical. Indeed, despite all mandates imposed throughout the world since the start of the 2020 pandemic, there continues to be outbreaks in hospitals of antibiotic-resistant *A. baumannii* infections, which represent a significant challenge in patient care.[38,39]

ACKNOWLEDGMENTS

This work was supported by NIH grant R35 GM134643 (H. M. H.).

CONFLICT OF INTEREST

The authors have no competing financial interests.

DATA AVAILABILITY STATEMENT

The data that support the findings of this study are openly available in Protein Data Bank at https://www.rcsb.org/.

REFERENCES

1. Falagas ME, Karveli EA. The changing global epidemiology of *Acinetobacter baumannii* infections: a development with major public health implications. *Clin Microbiol Infect*. 2007;13(2):117-119.
2. Lee CR, Lee JH, Park M, et al. Biology of *Acinetobacter baumannii*: pathogenesis, antibiotic resistance mechanisms, and prospective treatment options. *Front Cell Infect Microbiol*. 2017;7:55.
3. Cerqueira GM, Peleg AY. Insights into *Acinetobacter baumannii* pathogenicity. *IUBMB Life*. 2011;63(12):1055-1060.
4. Mancuso G, Midiri A, Gerace E, Biondo C. Bacterial antibiotic resistance: the most critical pathogens. *Pathogens*. 2021;10(10). https://mdpi-res.com/pathogens/pathogens-10-01310/article_deploy/pathogens-10-01310-v2.pdf
5. Alsan M, Klompas M. *Acinetobacter baumannii:* an emerging and important pathogen. *J Clin Outcomes Manag*. 2010;17(8):363-369.
6. Harding CM, Hennon SW, Feldman MF. Uncovering the mechanisms of *Acinetobacter baumannii* virulence. *Nat Rev Microbiol*. 2018;16(2):91-102.
7. Singh JK, Adams FG, Brown MH. Diversity and function of capsular polysaccharide in *Acinetobacter baumannii*. *Front Microbiol*. 2018;9:3301.
8. Russo TA, Luke NR, Beanan JM, et al. The K1 capsular polysaccharide of *Acinetobacter baumannii* strain 307-0294 is a major virulence factor. *Infect Immun*. 2010;78(9):3993-4000.
9. Kenyon JJ, Kasimova AA, Shashkov AS, Hall RM, Knirel YA. *Acinetobacter baumannii* isolate BAL_212 from Vietnam produces the K57 capsular polysaccharide containing a rarely occurring amino sugar *N*-acetylviosamine. *Microbiology (Reading)*. 2018;164(2):217-220.
10. Thoden JB, Reinhardt LA, Cook PD, Menden P, Cleland WW, Holden HM. Catalytic mechanism of perosamine *N*-acetyltransferase revealed by high-resolution X-ray crystallographic studies and kinetic analyses. *Biochemistry*. 2012;51(16):3433-3444.
11. Linehan MP, Thoden JB, Holden HM. Characterization of two enzymes from *Psychrobacter cryohalolentis* that are required for the biosynthesis of an unusual diacetamido-D-sugar. *J Biol Chem*. 2021;296:100463.
12. Thoden JB, Timson DJ, Reece RJ, Holden HM. Molecular structure of human galactokinase: implications for type II galactosemia. *J Biol Chem*. 2005;280(10):9662-9670.
13. Laskowski RA, MacArthur MW, Moss DS, Thornton JM. PROCHECK: a program to check the stereochemical quality of protein structures. *J Appl Cryst*. 1993;26:283-291.
14. Keegan RM, Winn MD. MrBUMP: an automated pipeline for molecular replacement. *Acta Crystallogr D Biol Crystallogr*. 2008;64(Pt 1):119-124.
15. Morrison MJ, Imperiali B. Biochemical analysis and structure determination of bacterial acetyltransferases responsible for the biosynthesis of UDP-*N*,*N*′-diacetylbacillosamine. *J Biol Chem*. 2013;288(45):32248-32260.
16. Emsley P, Cowtan K. Coot: model-building tools for molecular graphics. *Acta Crystallogr D Biol Crystallogr*. 2004;60(Pt 12 Pt 1):2126-2132.
17. Emsley P, Lohkamp B, Scott WG, Cowtan K. Features and development of coot. *Acta Crystallogr D Biol Crystallogr*. 2010;66(Pt 4):486-501.
18. Murshudov GN, Vagin AA, Dodson EJ. Refinement of macromolecular structures by the maximum-likelihood method. *Acta Crystallogr D Biol Crystallogr*. 1997;53(Pt 3):240-255.
19. Alpers DH, Appel SH, Tomkins GM. A spectrophotometric assay for thiogalactoside transacetylase. *J Biol Chem*. 1965;240:10-13.
20. Zimmer AL, Thoden JB, Holden HM. Three-dimensional structure of a sugar *N*-formyltransferase from *Francisella tularensis*. *Protein Sci*. 2014;23(3):273-283.
21. Olivier NB, Chen MM, Behr JR, Imperiali B. In vitro biosynthesis of UDP-*N*,*N*′-diacetylbacillosamine by enzymes of the *Campylobacter jejuni* general protein glycosylation system. *Biochemistry*. 2006;45(45):13659-13669.
22. Rangarajan ES, Ruane KM, Sulea T, et al. Structure and active site residues of PglD, an *N*-acetyltransferase from the Bacillosamine

synthetic pathway required for *N*-glycan synthesis in *Campylobacter jejuni*. *Biochemistry*. 2008;47(7):1827-1836.
23. Olivier NB, Imperiali B. Crystal structure and catalytic mechanism of PglD from *Campylobacter jejuni*. *J Biol Chem*. 2008;283(41):27937-27946.
24. Thoden JB, Cook PD, Schaffer C, Messner P, Holden HM. Structural and functional studies of QdtC: an *N*-acetyltransferase required for the biosynthesis of dTDP-3-acetamido-3,6-dideoxy-alpha-D-glucose. *Biochemistry*. 2009;48(12):2699-2709.
25. Thoden JB, Holden HM. Molecular structure of WlbB, a bacterial *N*-acetyltransferase involved in the biosynthesis of 2,3-diacetamido-2,3-dideoxy-D-mannuronic acid. *Biochemistry*. 2010;49(22):4644-4653.
26. Chantigian DP, Thoden JB, Holden HM. Structural and biochemical characterization of a bifunctional ketoisomerase/*N*-acetyltransferase from *Shewanella denitrificans*. *Biochemistry*. 2013;52(46):8374-8385.
27. Griffiths WA, Spencer KD, Thoden JB, Holden HM. Biochemical investigation of an *N*-acetyltransferase from *Helicobacter pullorum*. *Protein Sci*. 2021;30:2418-2432.
28. DeLano WL. Unraveling hot spots in binding interfaces: progress and challenges. *Curr Opin Struct Biol*. 2002;12(1):14-20.
29. Ray WJ Jr, Puvathingal JM. A simple procedure for removing contaminating aldehydes and peroxides from aqueous solutions of polyethylene glycols and of nonionic detergents that are based on the polyoxyethylene linkage. *Anal Biochem*. 1985;146(2):307-312.
30. Strominger JL, Scott SS. Isolation of thymidine diphosphosugar compounds from *Escherichia coli*. *Biochim Biophys Acta*. 1959;35:552-553.
31. Katzenellenbogen E, Romanowska E, Kocharova NA, Knirel YA, Shashkov AS, Kochetkov NK. The structure of a glycerol teichoic acid-like O-specific polysaccharide of *Hafnia alvei* 1205. *Carbohydr Res*. 1992;231:249-260.
32. Zatonskii GV, Kocharova NA, Katzenellenbogen E, Shashkov AS, Knirel YA. NMR spectroscopic elucidation of the structure of a glycerol teichoic acid-like O-specific polysaccharide of the bacterium *Hafnia alvei* strain PCM 1199. *Biochemistry (Mosc)*. 1997;62(12):1448-1453.
33. Haseley SR, Holst O, Brade H. Structural studies of the O-antigen isolated from the phenol-soluble lipopolysaccharide of *Acinetobacter baumannii* (DNA group 2) strain 9. *Eur J Biochem*. 1998;251(1-2):189-194.
34. Zdorovenko GM, Gvozdiak RI, Gubanova N, Afonina GB, Zdorovenko EL. Characteristics of lipopolysaccharide from *Pseudomonas fluorescens* (biovar I). *Mikrobiologiia*. 1999;68(3):330-339.
35. Tomshich SV, Kokoulin MS, Kalinovsky AI, Nedashkovskaya OI, Komandrova NA. Structure of the O-specific polysaccharide from a marine bacterium *Cellulophaga tyrosinoxydans*. *Carbohydr Res*. 2015;413:1-4.
36. Pakiet K, Turska-Szewczuk A, Karas MA, Pekala A, Pietras H. Structure of the O-specific polysaccharide from the lipopolysaccharide of *Aeromonas hydrophila* strain K691 containing 4-acetamido-4,-6-dideoxy-D-glucose. *Carbohydr Res*. 2017;439:23-29.
37. Wang Y, Xu Y, Perepelov AV, et al. Biochemical characterization of dTDP-D-Qui4N and dTDP-D-Qui4NAc biosynthetic pathways in *Shigella dysenteriae* type 7 and *Escherichia coli* O7. *J Bacteriol*. 2007;189(23):8626-8635.
38. Russo A, Gavaruzzi F, Ceccarelli G, et al. Multidrug-resistant *Acinetobacter baumannii* infections in COVID-19 patients hospitalized in intensive care unit. *Infection*. 2022;50(1):83-92.
39. Thoma R, Seneghini M, Seiffert SN, et al. The challenge of preventing and containing outbreaks of multidrug-resistant organisms and *Candida auris* during the coronavirus disease 2019 pandemic: report of a carbapenem-resistant *Acinetobacter baumannii* outbreak and a systematic review of the literature. *Antimicrob Resist Infect Control*. 2022;11(1):12.

How to cite this article: Herkert NR, Thoden JB, Holden HM. Structure and function of an *N*-acetyltransferase from the human pathogen *Acinetobacter baumannii* isolate BAL_212. *Proteins*. 2022;90(8):1594-1605. doi:10.1002/prot.26334